J Appl Electrochem (2008) 38:507–514
DOI 10.1007/s10800-007-9465-3

ORIGINAL PAPER

Carbon nanocapsules as an electrocatalyst support for the oxygen reduction reaction in alkaline electrolyte

Y. M. Lin · Y. M. Chang · P. W. Wu · P. Lin · Y. Y. Li · C. Y. Wu · C. F. Tsai · K. Y. Yeh

Received: 2 July 2007 / Revised: 26 November 2007 / Accepted: 28 November 2007 / Published online: 8 December 2007

Abstract Carbon Nanocapsules (CNCs) were investigated for their electrocatalytic performances for the oxygen reduction reaction in alkaline electrolyte. With an average diameter of 10–30 nm, the CNCs are composed of graphene layers encapsulating a hollow core. A gas diffusion electrode (GDE) made of CNCs revealed a much enhanced *i*–V polarization response than that of Vulcan XC72. However, its performance was moderately lower than that of Black Pearls 2000. In addition, the CNCs were impregnated with nanoparticles of Ag, MnO_x and CoO_x. The *i*–V and galvanostatic results of the catalyzed CNCs indicated significant improvements over that of noncatalyzed CNCs. For example, a Ag–CNC derived GDE was capable of delivering 1.03 and 0.88 V at current densities of 100 and 200 mA cm^{-2}, respectively. Our study offers direct evidence that the CNCs not only exhibit unique electrocatalytic abilities but also function superbly as an electrocatalyst support.

Keywords Alkaline fuel cell · Carbon nanocapsules · Gas diffusion electrode · Electrocatalyst · Oxygen reduction reaction

1 Introduction

Fuel cells and metal air batteries are expected to play significant roles as clean energy alternatives to ameliorate the worsening greenhouse effect [1, 2]. For both systems, the oxygen reduction reaction (ORR) is the critical electrochemical step responsible for the majority of electrode polarization loss [3]. Many materials have been investigated as an electrocatalyst to enhance the ORR. They include metals (Pt, Ag) [4–9], metal oxides (RuO_2, MnO_2, CoO) [10–12], perovskites ($LaCoO_3$, $La_{0.6}Ca_{0.4}CoO_3$) [13–17], spinels ($Ni_xAl_{1-x}Mn_2O_4$, $Ni_2Co_2O_4$, $Mn_{3x}Co_{3-3x}O_4$) [18–20], as well as pyrolyzed N-4 chelate compounds (CoTMPP) [21]. A thorough review was provided recently by Wang, discussing available non-platinum electrocatalysts [22].

The ORR proceeds in distinct steps contingent on the electrolyte used. In an alkaline solution, the ORR occurs via a direct four electron pathway or a two electron peroxide route listed below. In the four electron pathway (1), the oxygen molecule is reduced to hydroxyl ion in a single step;

$$O_2 + 2H_2O + 4e^- \rightarrow 4OH^- \quad E^o = 0.401V \tag{1}$$

In contrast, in the two electron route, the oxygen molecule is reduced first to HO_2^- peroxide ion (2), followed by further reduction to hydroxyl ion (3), or decomposition to form hydroxyl ion and oxygen (4).

$$O_2 + H_2O + 2e^- \rightarrow HO_2^- + OH^- \quad E^o = -0.065V \tag{2}$$

$$HO_2^- + H_2O + 2e^- \rightarrow 3OH^- \quad E^o = 0.867V \tag{3}$$

$$2HO_2^- \rightarrow 2\ OH^- + O_2 \tag{4}$$

Electrocatalysts that reduce oxygen through the four electron pathway are preferred because less electrode polarization is expected.

A gas diffusion electrode (GDE) is required for fuel cells and metal air batteries. The GDE is a porous platform incorporating current collector, hydrophobic PTFE resin

Y. M. Lin · Y. M. Chang · P. W. Wu (✉) · P. Lin · C. Y. Wu · C. F. Tsai · K. Y. Yeh
Department of Materials Science and Engineering, National Chiao Tung University, Hsin-Chu 300, Taiwan, ROC
e-mail: ppwu@mail.nctu.edu.tw

Y. Y. Li
Department of Chemical Engineering, National Chung Cheng University, Chia-Yi 621, Taiwan, ROC

and carbonaceous material impregnated with catalytic nanoparticles [23, 24]. The porosity, pore structure and hydrophobicity of the GDE are carefully designed to allow an extensive reaction interface between the gaseous oxygen and liquid electrolyte in the vicinity of the electrocatalyst. To date, it is recognized that the GDE is the crucial component enabling successful implementation of fuel cells and metal air batteries.

Many carbonaceous materials have been investigated as possible electrocatalyst supports [25–27]. They range from conventional carbon powders such as Vulcan XC72, Black Pearls, Shawiningan Blacks and active carbons, to less familiar ones including glassy carbons, carbon fibers and hard carbon spherules [28–30]. A detailed discussion was recently provided by Dicks [31]. With recent progress in the synthesis of nanostructured materials, exotic forms of carbon such as carbon nanotubes (CNTs) and carbon nanocapsules (CNCs) have been reported [32, 33]. It is established that the CNTs exhibit extraordinary mechanical strength, excellent electronic and thermal conductivity, as well as chemical stability and high surface area. These are desirable physical properties for electrocatalyst supports. Hence, the CNTs' applicability as an electrocatalyst support has received much attention recently. For example, Kongkanand et al. observed significant enhancements in the electrocatalytic activities of single-walled CNTs decorated with Pt nanoparticles [34]. A similar result was reported by Che et al. and they attributed the enhanced capabilities to the accessible inner surface of CNTs [35]. In addition, the strategy of hybrid carbonaceous materials has been explored. Huang et al. mixed active carbons with the CNTs and observed substantial improvements in electrocatalytic performance once Pt was loaded [36].

On the other hand, research focusing on the CNCs as electrocatalyst supports has not been reported yet. In this work, nanoparticles of Ag, MnO_x and CoO_x were synthesized and embedded in the CNCs to fabricate GDEs. Material characterization and electrochemical analysis were conducted to determine the intrinsic catalytic power of CNCs as well as their applicability as an electrocatalyst support.

2 Experimental

2.1 Preparation and characterization of CNCs and catalyzed CNCs

The synthesis of CNCs employed a flame combustion approach with feedstock of C_2H_2 and O_2. At an appropriate ratio of C_2H_2/O_2, the CNCs were formed in the incomplete combustion region of the flame and collected from the chamber upon cooling. On average, the diameter of the as-synthesized CNCs ranged between 10 and 30 nm with slightly irregular shapes. Detailed synthesis parameters and equipment involved were reported by us previously [33].

For study of CNCs as an electrocatalyst support, the CNCs were impregnated with known electrocatalysts such as Ag, MnO_x and CoO_x. The impregnation process entailed a typical wet-chemical approach to produce nanoparticles of Ag, MnO_x and CoO_x distributed uniformly within the CNCs. Initially, 3.0 g of CNCs was mixed in 30 ml of 5 wt% Triton X-100 (Sigma-Aldrich 98%) aqueous solution to prepare the standard CNC dispersion. In synthesis of CNCs embedded with Ag nanoparticles, 1.54 g of $AgNO_3$ (SHOWA 99.8% purity) was first dissolved in 10 ml of deionized water. After complete dissolution, the silver salt solution was mixed with 30 ml of the standard CNC dispersion for 1 h. Then, 8.4 ml of HCl solution (1.19 M) was added to the mixture to induce precipitation of AgCl. The mixture was stirred for 6 h ensuring complete reaction of Ag^+ and Cl^-. Next the mixture was dried at 70 °C for 48 h followed by a reduction treatment (H_2 5%–N_2 95%) at 700 °C for 4 h to form Ag–CNC powders.

For synthesis of MnO_x–CNC, 3.0 g of $KMnO_4$ (SHOWA 99.3%) was dissolved in 10 ml of deionized water and then mixed with 30 ml of the standard CNC dispersion. Subsequent processes involved oven drying at 70 °C for 48 h and heat treatment at 800 °C for 4 h in N_2 environment to initiate formation of nanoparticulate MnO_x. Upon cooling to room temperature, the MnO_x–CNC powders were washed with excess deionized water to remove residual potassium oxides. For production of CoO_x–CNC, 4.94 g of $Co(NO_3)_2$ (J.T. Baker 99.1%) was first dissolved in 10 ml of deionized water and mixed with 30 ml of the standard CNC dispersion. Then the mixture was oven dried at 70 °C for 48 h followed by heat treatment at 800 °C for 4 h in N_2 atmosphere.

2.2 Fabrication and electrochemical characterization of GDEs

Once the CNCs were decorated with desirable electrocatalysts, the next step was to fabricate GDEs for electrochemical characterizations. The construction of GDE started from preparation of the gas diffusion layer (GDL) where 0.80 g of active materials (Ag–CNC, MnO_x–CNC or CoO_x–CNC) was dispersed thoroughly in 15 ml of ethanol (95% purity) for 30 s in a high speed mixer. In addition, 0.33 g of 60 wt% polytetrafluoroethylene (PTFE) resin (Dupont-T30) was diluted in 15 ml of ethanol. Then both dispersions were added together followed by intense mixing for 3 min to form a dough-like paste. With repeated rolling and kneading, the paste was pressed into a GDL ($\sim$0.20 mm in thickness) with appropriate elasticity. The second step was to laminate the

GDL with a nickel foam at a pressure of 685 psi. Finally, the GDE was heat treated at 350 °C for 10 min in air to drive out residual ethanol and surfactant. The thickness of the finished GDE was about 0.38 mm. Excluding the current collector, the material loading of the GDE was about 0.05 g cm^{-2}, of which 0.04 g cm^{-2} was the active material (catalyst-CNC) and 0.01 g cm^{-2} was the PTFE. Figure 1 provides the flow chart detailing the GDE fabrication steps.

As electrochemical reaction is an interfacial phenomenon, the surface area of the electrode materials is a critical factor. For accurate comparison of the intrinsic ORR of the CNCs, typical Vulcan XC-72 (XC72: 254 m^2 g^{-1}) and Black Pearls 2000 (BP2000: 1,500 m^2 g^{-1}) from Cabot Inc. were used following the identical steps mentioned above. Their electrochemical performances were measured against that of CNCs (333 m^2 g^{-1}).

Electrochemical characterizations for the GDEs were conducted in *i*–V polarizations and galvanostatic measurements using a Solartron 1287 potentiostat. An arrangement of three electrode cell was adopted in which the GDE was used as the working electrode, Ti mesh coated with RuO_2/IrO_2 as the counter electrode, and Zn rod (99.98%) as the reference electrode. The Zn rod was used for quick determination of the operating voltage of a functional Zn-Air cell. The KOH solution (30 wt%) was used as electrolyte. During measurements, the backside of the GDE ($\sim$3 cm^2) was exposed to ambient air. The scan rate for the *i*–V polarizations was set at 1 mV s^{-1}. Galvanostatic measurements were conducted at current densities from 10 to 200 mA cm^{-2} for 10 min.

A TEM (JEOL JEM-2010) was used to observe the microstructure of the as-synthesized CNCs. X-ray (Bede D1, Cu K_α = 1.54 Å) was employed to identify relevant phases present for Ag–CNC, MnO_x–CNC and CoO_x–CNC. A SEM (Hitachi JSM 6700F) was applied to evaluate the morphologies and microstructures of GDLs.

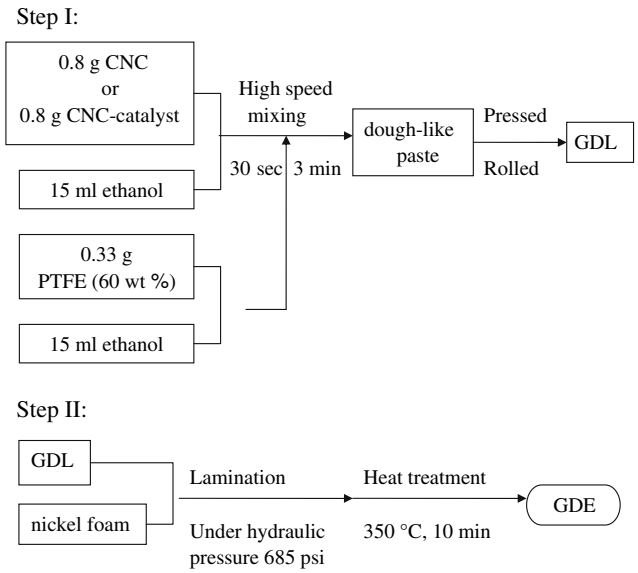

Fig. 1 Flow chart of processing steps involved in the GDE fabrication

3 Results and discussion

3.1 Characterization of CNCs as an electrocatalyst

A high resolution TEM image of the as-synthesized CNCs is presented in Fig. 2a. It can be seen that the CNCs exhibited a core-shell microstructure with graphene layers on the perimeter encompassing an empty core. The diameter of the CNCs is approximately 10 nm while the

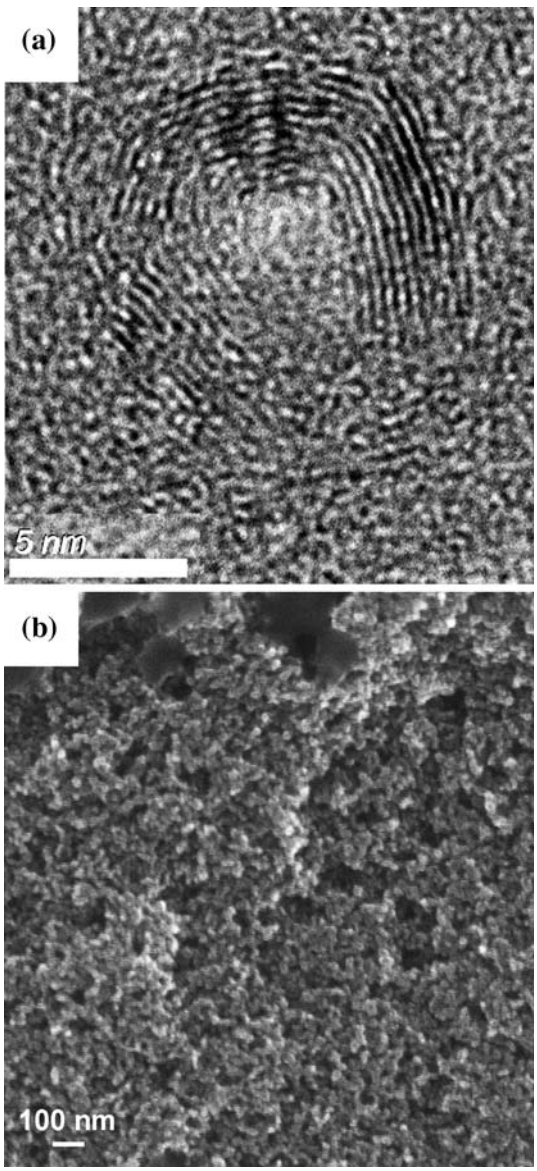

Fig. 2 Images of the CNCs from (**a**) HR-TEM and (**b**) SEM

diameter of the core is nearly 5 nm. Previous study using the Raman analysis revealed that the ratio of the G-band/D-band was 0.7, a value similar to that of multi-walled carbon nanotubes (MWCNTs) [33]. Because catalysts were not used in the flame combustion stage, EDS analysis of the resulting CNCs indicated impressive purity. In contrast, typical carbon powders always contain minute amounts of impurities labelled as the ash content. Fig. 2b demonstrates a SEM image of the as-synthesized CNCs. Apparently the CNCs aggregated into a highly porous structure but individual CNC particles were rather uniform in sizes.

Since the as-synthesized CNCs were uniform in size with graphene layers on the perimeter, they showed considerable potential as an electrocatalyst support in GDE technologies. Common wisdom has established that the size uniformity is particularly favored for dense packing. In addition, the graphene layers on the perimeter confer enhanced electrical conductivity. Besides, the hollow core of the CNCs suggest a reduced density, making it possible for GDEs with higher specific energy (W g^{-1}). Lastly, the as-synthesized CNCs were recorded with a surface area of 333 m^2 g^{-1} from BET measurement, a value considered desirable for the following process developments.

Powders of CNCs, XC72 and BP2000 were used in the dough rolling process to fabricate the GDLs to determine their intrinsic electrocatalytic abilities. Figure 3 demonstrates their *i*–V polarization behavior. For the CNC derived GDE, the voltage started around 1.14 V and decreased with increasing current density. Likewise, for the XC72 and BP2000 derived GDEs the voltage began at 0.99 and 1.26 V, respectively, and decreased as expected with increasing current density. The CNC-derived GDE was capable of sustaining 0.81 and 0.68 V at discharging current densities of 100 and 200 mA cm^{-2}, respectively. These values were an impressive 80–90 mV increase over

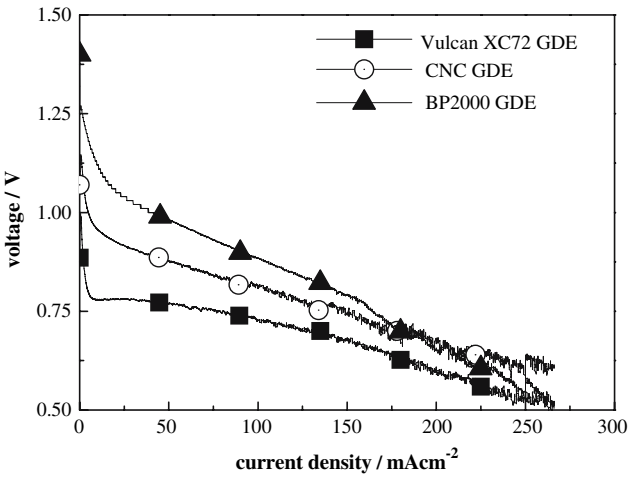

Fig. 3 The *i*–V polarization curves of the noncatalyzed GDEs from CNCs, XC72 and BP2000, respectively

those of XC72, of which voltages of 0.72 and 0.60 V were obtained at identical current densities. In contrast, the BP2000 derived GDE was capable of delivering 0.88 and 0.65 V at current densities of 100 and 200 mA cm^{-2}, respectively. At current densities below 175 mA cm^{-2}, the BP2000 derived GDE demonstrated a moderately better performance than that of CNC derived GDE. However, its superiority decreased rapidly with increasing current density. The discrepancy in electrocatalytic performances can be attributed to the difference in effective surface area. Generally speaking, particles of higher surface area are likely to produce GDEs with larger effective interfaces. The surface areas of CNCs and BP2000 represented 31 and 490% increments over that of XC72. We believe that the enhanced *i*–V response of CNCs is partly attributed to their intrinsic high surface area. This argument was further supported by pore size measurements in which the majority of the pores for the CNC derived GDE, XC72 derived GDE and BP200 derived GDE were 0.068, 0.187 and 0.153 μm, respectively. In contrast, the effect of surface area on the *i*–V performance from BP2000 was not so pronounced. This suggests the CNCs possess unique electrocatalytic abilities.

3.2 Characterization of CNCs as an electrocatalyst support

In alkaline solution, carbon is known to be an effective electrocatalyst via the two electron route [37]. Unfortunately, excess accumulation of peroxide ions is believed to accelerate oxidation of the carbon substrate which often results in premature electrode failure. Therefore, mixing with particular peroxide decomposing catalysts such as Ag, MnO_2 and Ni–Co spinels was suggested to prolong the stability of GDEs [37]. Previously, powder mixtures of Ag and CNCs were shown to reveal promising ORR abilities [38]. In this study, impregnation of CNCs with known electrocatalysts was carried out to further explore CNCs' potential as an electrocatalyst support. The electrocatalysts selected were Ag, MnO_x and CoO_x. Synthesis of electrocatalytic nanoparticles supported on carbonaceous materials have been reported extensively [39, 40]. In our case, the weight ratios of Ag:CNC, Mn:CNC and Co:CNC were kept at 1:3.

X-ray results of the Ag–CNC, MnO_x–CNC and CoO_x–CNC are provided in Fig. 4. The broad peak around 25° was derived from the CNCs. Clearly exhibited in the diffraction patterns, well crystallized Ag in FCC phase was observed for Ag–CNC powders. In our formulation, the concentrations of Ag^+ and Cl^- were 0.16 and 1.77 M, respectively. Multiplication of these concentrations gives a value that is much greater than the solubility limit of AgCl,

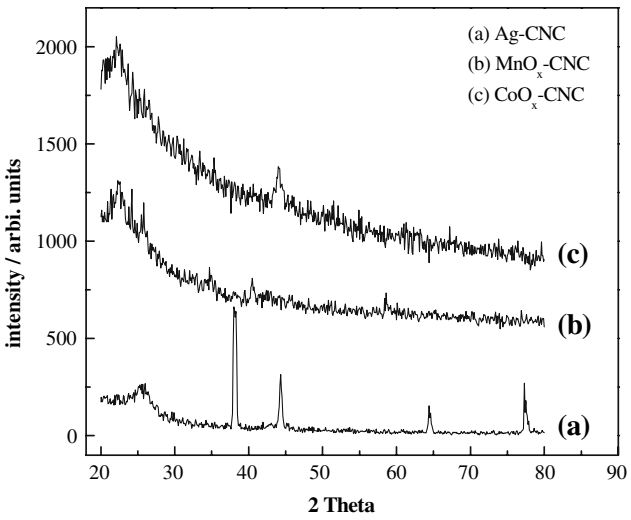

Fig. 4 X-ray results of the as-synthesized powders; (**a**) Ag–CNC, (**b**) MnO_x–CNC and (**c**) CoO_x–CNC

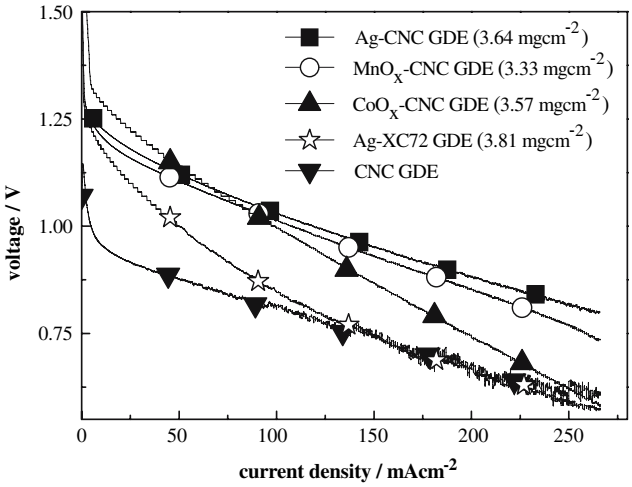

Fig. 5 The *i*–V polarization curves of the CNC derived GDE and the catalyzed GDEs with electrocatalysts of Ag–CNC, MnO_x–CNC, CoO_x–CNC and Ag–XC72

$\sim 1.6 \times 10^{-10}$ mol^2 l^{-2} [41]. Therefore, spontaneous precipitation of AgCl was expected to occur once the HCl was added. In subsequent heat treatment, the AgCl was successfully reduced forming crystalline Ag particles. In contrast, X-ray patterns for the MnO_x–CNC powders exhibited mixed oxidation states for Mn ions. The strongest peaks of 22.5° and 24.2° were from the (110) of MnO_2 and (131) of Mn_2O_7, respectively. Furthermore, peaks at 40.5° and 58.4° were identified as the (200) from MnO and the (321) from Mn_3O_4, respectively. In contrast, the X-ray pattern of CoO_x–CNC demonstrated an amorphous nature with singular peak at 44.2°, which was attributed to the (400) of Co_3O_4. As a result, the exact natures and chemical compositions of MnO_x and CoO_x cannot be determined conclusively. It is likely that either a decomposition temperature of 800 °C for 4 h was insufficient to form well-crystallized MnO_x and CoO_x particles, or additional oxygen was necessary to compensate the loss by volatile NO_x during heat treatment. We did not carry out reduction treatments for both MnO_x–CNC and CoO_x–CNC because previous studies linked electrocatalytic abilities to oxides of Mn and Co [42, 43].

Electrocatalytic performances of Ag–CNC, CoO_x–CNC and MnO_x–CNC were evaluated by comparing their *i*–V characteristics against that of noncatalyzed CNCs. Fig. 5 exhibits the results with the loading amounts listed. As clearly demonstrated, Ag–CNC exhibited the highest electrocatalytic performance among these samples. It was capable of delivering 1.12 V at 50 mA cm^{-2} and maintaining a respectable 0.88 V at 200 mA cm^{-2}. Similarly, the MnO_x–CNC exhibited slightly lower capabilities, delivering voltages of 1.11 V at 50 mA cm^{-2} and 0.85 V at 200 mA cm^{-2}, respectively. In contrast, the CoO_x–CNC demonstrated the poorest electrocatalytic behavior among these three, exhibiting 1.12 V at 50 mA cm^{-2} and 0.74 V at 200 mA cm^{-2}, respectively. Nevertheless, its performance still represented notable enhancements over that of noncatalyzed CNCs. Also shown is the Ag–XC72 derived GDE where its performance is lower than that of Ag–CNC derived GDE by 200 mV. These results not only confirm general applicability of CNCs as an electrocatalyst support but also suggest unique intrinsic abilities of CNCs.

Figure 6 presents the SEM pictures of GDL from (a) Ag–CNC, (b) MnO_x–CNC and (c) CoO_x–CNC. Shown in Fig. 6a, the particles labelled as Ag ranged between 150 and 250 nm in spherical shapes. They were dispersed uniformly and coalescence of Ag particles was not observed. In Fig. 6b, the MnO_x existed in polyhedrons of 125 nm in size. In contrast coalescence of these MnO_x particles seems to take place to some degree. Figure 6c presents the picture of CoO_x–CNC showing CoO_x in the form of elongated polyhedrons of 80 nm without coalescence. After loadings of nanoparticulate Ag, MnO_x and CoO_x, the effective surface areas were reduced to 275, 99 and 298 m^2 g^{-1}, respectively.

We were also interested in the effect of material loading as this determined not only electrocatalytic abilities but also physical characteristics such as microstructure, hydrophobicity and porosity of the resulting GDEs. Excluding the weight of Ni foam, the GDE contained 80 wt% Ag–CNC and 20 wt% PTFE. Since the weight ratio of Ag to CNC was 1:3, the net Ag loading of the GDE was 20 wt%. With a reduced $AgNO_3$ amount in the CNC dispersion, we prepared the GDE with a net Ag loading of 13 wt%. Comparison of the respective electrochemical performances is shown in Fig. 7. The *i*–V relations were as expected, as a lower amount of Ag–CNC resulted in a considerable reduction in electrocatalytic ability,

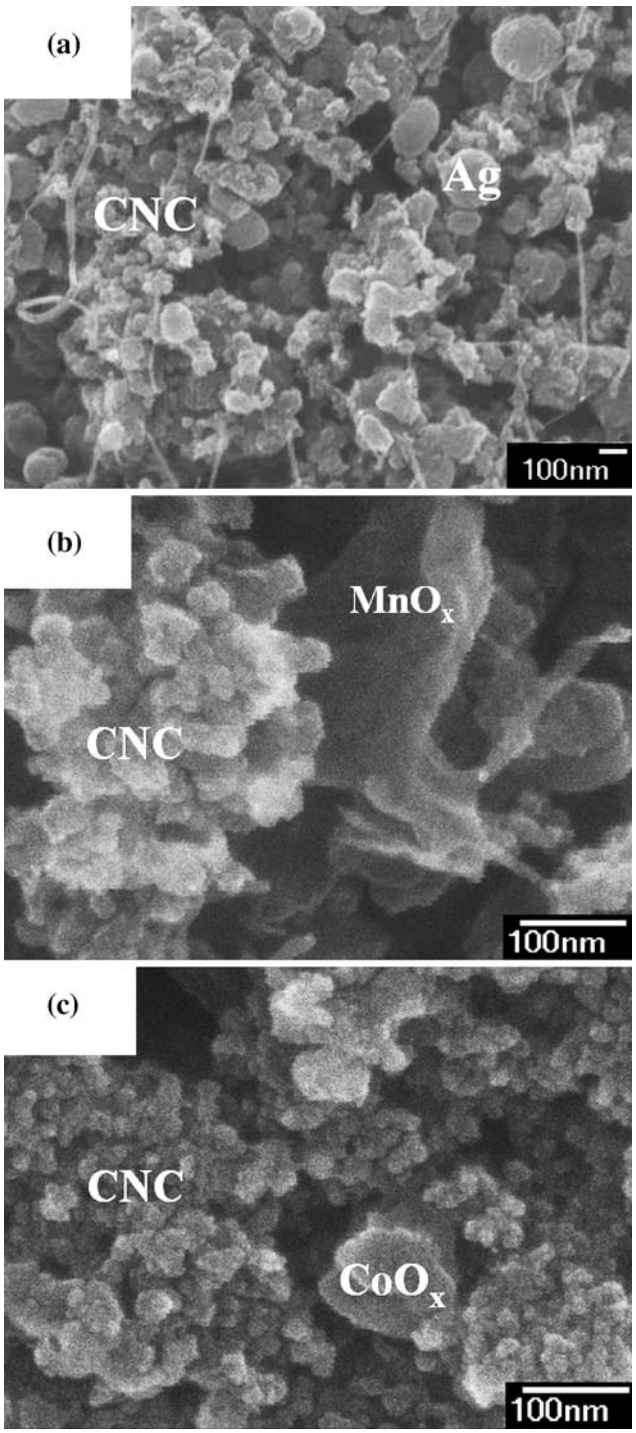

Fig. 6 SEM pictures of the GDLs from (**a**) Ag–CNC, (**b**) MnO_x–CNC and (**c**) CoO_x–CNC

particularly at high current density. However, the differences were negligible at current densities below 50 mA cm^{-2}. These *i*–V curves were much better than that of noncatalyzed CNCs. This suggested that further optimization of the material loading is possible to obtain desirable performances at reasonable cost. In addition, the

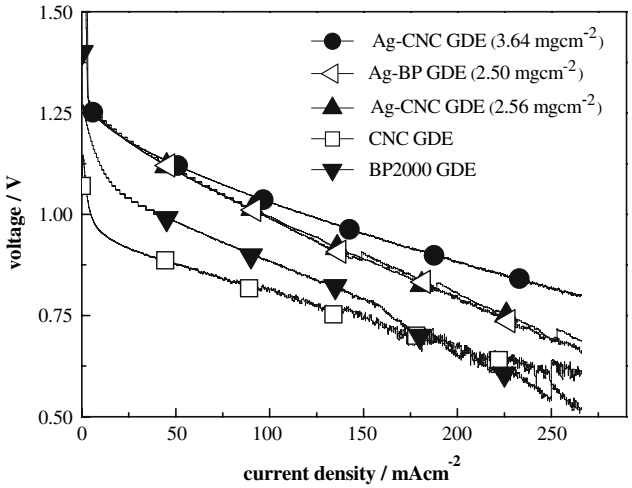

Fig. 7 The *i*–V polarization curves of GDEs catalyzed by CNCs, Ag–CNC and Ag–BP2000

i–V curve of Ag–BP2000 derived GDE is also shown. The result for the Ag–BP2000 GDE was comparable to that of Ag–CNC GDE at similar electrocatalyst loadings. This is especially encouraging as high surface area carbon powders like BP2000 present substantial processing difficulties in GDE fabrication. Our result indicates that CNCs can function equally as well as BP2000 as electrocatalyst supports.

Once the performance of the catalyzed-CNCs was established through *i*–V polarization studies, the next step was to explore their discharge behavior galvanostatically to determine their lifetime and stability. The current densities under study ranged from 10 to 200 mA cm^{-2}. Figure 8 presents the results for the GDEs with (a) Ag–CNC, (b) MnO_x–CNC and (c) CoO_x–CNC. The voltage readings in galvanostatic discharge were consistent with those observed from earlier *i*–V polarizations. With a timeframe of 10 min, the voltage profiles revealed rather stable and sustainable discharging behavior. We realize that 10 min of testing is limited and we are currently exploring galvanostatic discharges for longer timeframes to identify possible degradation mechanisms.

4 Conclusions

The CNCs were synthesized and characterized for their intrinsic electrochemical abilities and prospects as an electrocatalyst support. The as-synthesized CNCs exhibited a uniform size distribution of 10–30 nm. Impregnations of the CNCs with electrocatalysts were carried out using wet-chemical methods where nanoparticulate Ag, MnO_x and CoO_x were evenly embedded within the CNCs aggregates. A dough-rolling technique was employed to prepare an appropriate GDE structure for both *i*–V polarizations and

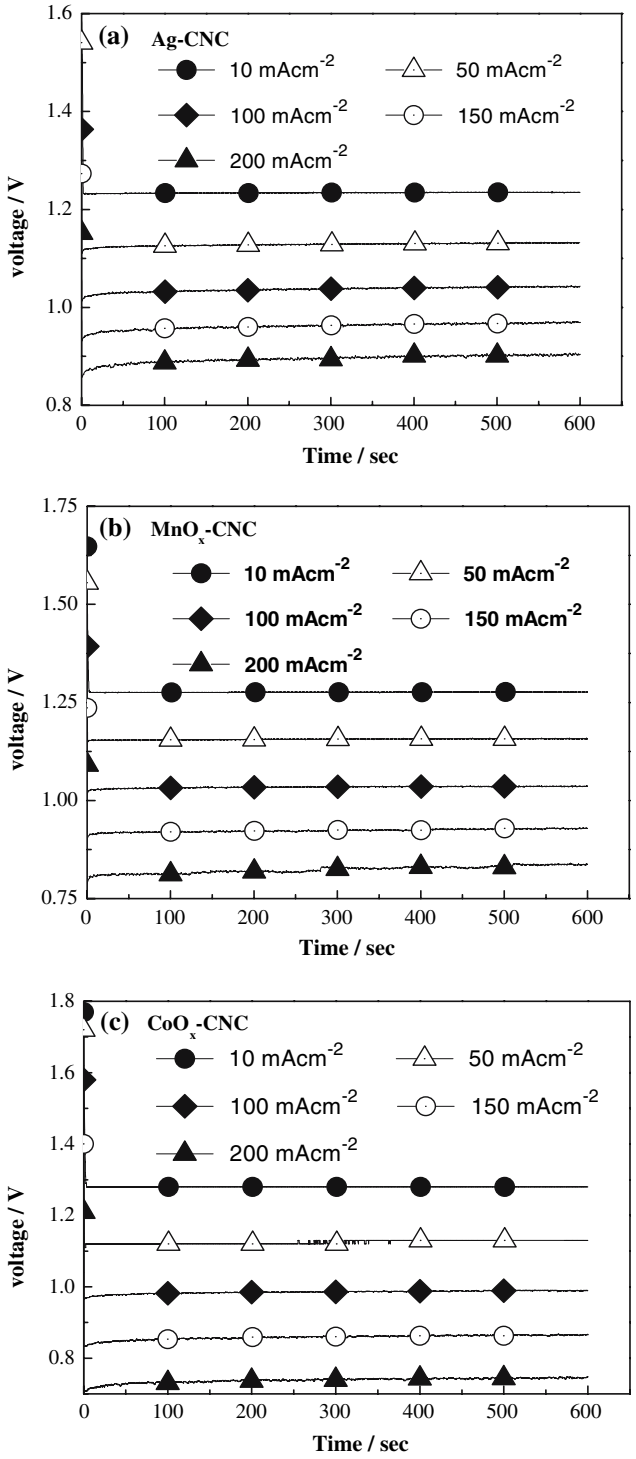

Fig. 8 Galvanostatic discharge profiles of the GDEs catalyzed by (**a**) Ag–CNC, (**b**) MnO_x–CNC and (**c**) CoO_x–CNC for current densities from 10 to 200 mA cm^{-2}

galvanostatic measurements. In *i*–V polarizations of the GDEs from CNCs, XC72 and BP2000, the CNCs behaved much better than that of XC-72, reflecting a unique intrinsic electrocatalytic ability. After loadings with electrocatalysts, their *i*–V responses demonstrated significant enhancements over that of noncatalyzed CNCs. For example, the Ag–CNC derived GDE was capable of delivering 1.03 and 0.88 V at current densities of 100 and 200 mA cm^{-2}, respectively. Profiles from the galvanostatic discharges confirmed that the Ag–CNC, MnO_x–CNC and CoO_x–CNC were stable and sustainable. The enhanced electrocatalytic performance of the CNCs is attributable to their large surface area and uniformity in size. Our results offer strong evidence that CNCs are excellent supports for electrocatalysts.

Acknowledgements Taiwan Power Company provided financial support for this research. Equipment loan from Professor George Tu is especially noted. Thanks are due for Yu-Zhen Hsing and Ting-Yu Chang for their assistances in many tasks.

References

1. Steele BCH, Heinzel A (2001) Nature 414:345
2. Arai H, Müller S, Haas O (2000) J Electrochem Soc 147:3584
3. Yeager E (1986) J Mol Catal 38:5
4. Li X, Hsing IM (2006) Electrochim Acta 51:5250
5. Lafuente E et al (2006) J Mater Res 21:2841
6. Ding J, Chan KY, Ren J, Xiao FS (2005) Electrochim Acta 50:3131
7. Gamburzev S, Petrov K, Appleby AJ (2002) J Appl Electrochem 32:805
8. Chou KS, Ren CY (2000) Mater Chem Phys 64:241
9. Tang Z, Liu S, Dong S, Wang E (2001) J Electroanal Chem 502:146
10. Ardizzone S, Falciola M, Trasatti S (1989) J Electrochem Soc 136:1545
11. Bagotzky VS, Shumilova NA, Khrushcheva EI (1975) Electrochim Acta 21:919
12. Wei ZD, Huang WZ, Zhang ST, Tan J (2000) J Appl Electrochem 30:1133
13. Tiwari SK, Chartier P, Singh RN (1995) J Electrochem Soc 142:148
14. Müller S, Striebel K, Haas O (1994) Electrochim Acta 39:1661
15. Wu NL, Liu WR, Su SJ (2003) Electrochim Acta 48:1567
16. Lee CK, Striebel KA, McLarnon FR, Cairns EJ (1997) J Electrochem Soc 144:3801
17. Bockris JOM, Otagawa T (1984) J Electrochem Soc 131:290
18. Ponce J, Rehspringer JL, Poillerat G, Gautier JL (2001) Electrochim Acta 46:3373
19. Sugawara M, Ohno M, Matsuki K (1997) J Mater Chem 7:833
20. Baydi ME, Tiwari SK, Singh RN et al (1995) J Solid State Chem 116:157
21. Zhao F, Harnisch F, Schröder U, Scholz F, Bogdano P, Herrmann I (2005) Electrochem Commun 7:1405
22. Wang B (2005) J Power Sources 152:1
23. Maja M, Orecchia C, Strano M, Tosco P, Vanni M (2000) Electrochim Acta 46:423
24. Litster S, McLean G (2004) J Power Sources 130:61
25. Tomantschger K, Findlay R, Hanson M, Kordesch K, Srinivasan S (1992) J Power Sources 39:21
26. Staud N, Ross PN (1986) J Electrochem Soc 133:1079
27. Ross PN, Sattler M (1988) J Electrochem Soc 135:1464
28. Schmid TJ, Gasteiger HA, Behm RJ (1999) J Electrochem Soc 146:1296

29. Nadeau G, Song XY, Masse M, Guerfi A, Brisard G, Kinoshita K, Zaghib K (2002) J Power Sources 108:86
30. Yang R, Qiu X, Zhang H et al (2005) Carbon 43:11
31. Dicks AL (2006) J Power Sources 156:128
32. Iijima S (1991) Nature 354:56
33. Liu TC, Li YY (2006) Carbon 44:2045
34. Kongkanand A, Kuwabata S, Girishkumar G, Kamat P (2006) Langmuir 22:2392
35. Che G, Lakshmi BB, Fisher ER (1998) Nature 393:346
36. Huang H, Zhang W, Li M, Gan Y, Chen J, Kuang Y (2005) J Colloid Interface Sci 284:593
37. Kinoshita K (1988) Carbon. John Wiley & Sons, New York
38. Wu CY, Wu PW, Lin P, Li YY, Lin YM (2007) J Electrochem Soc 154:B1059
39. Cao YL, Yang HY, Ai XP, Xiao LF (2003) J Electroanal Chem 557:127
40. Yang Y, Zhou Y (1995) J Electroanal Chem 397:271
41. Skoog DA, West DM, Holler FJ (1996) Fundamentals of analytical chemistry. Saunders College Pub, Philadelphia
42. Yang J, Xu JJ (2003) Electrochem Commun 5:306
43. Jiang SP, Tseung ACC (1990) J Electrochem Soc 137:3442